Supporting Information

$LiFePO_4$ mesocrystals coated with N-doped carbon from ionic liquids for Li-ion batteries

Congjie Lv,[a] Xiaochuan Duan,*[a] Jiwei Deng[a] and Taihong Wang[a]

S1. Experimental Section

Materials. 1-n-butyl-3methylimidazolium digydrogenphosphate ([Bmim][H_2PO_4]) and *N*-methyl-*N*-propylpyrrolidinium bis(trifluoromethyl sulfonyl)imide ($PYR_{14}TFSI$) were obtained from Lanzhou Greenchem ILS, LICP. CAS. China. Other chemicals were purchased and used without further purification. The water was deionized before use.

Synthesis of ferric giniite hexadecahedra. In a typical synthesis[1], [Bmim][H_2PO_4] (5 mmol, 1.18 g) was put into a mixed solution (15 mL) of methanol and ethylene glycol (V(CH_3OH):V(EG) = 1:2) under stirring to form a homogenous solution. Subsequently, $Fe(NO_3)_3 \cdot 9H_2O$ (2.5 mmol, 1.01 g) was added into the above homogenous solution under continuous stirring. Hydrochloric acid (HCl, 10 M) was added dropwise until the pH value of the mixture reached 2. After stirring for 10 min, the total solution was transferred into a stainless-steel autoclave with a capacity of 20 mL, sealed and heated at 180 °C for 12 h.

Synthesis of C,N-LFP mesocrystals. When the reaction was complete, the autoclave was cooled to room temperature naturally. The resultant product was filtered and collected, and then transferred into 15 mL of EG under stirring. Subsequently, $LiCl \cdot H_2O$ (2.0 mmol, 0.12 g) was added into the above solution under continuous stirring. After stirring for 30 min, the total solution was transferred into a stainless-steel autoclave with a capacity of 20 mL, sealed and heated at 220 °C for 48 h. After cooling naturally to ambient temperature, the resultant product was collected and washed with deionized water and anhydrous ethanol for three times. In the next step, the obtained product was mixed with 0.5 mL of $PYR_{14}TFSI$ and afterwards decomposed at 300 °C under nitrogen atmosphere for 3 h. Then the precalcinated sample was ground and heated at 700 °C for 4 h under nitrogen atmosphere to obtain the final product.

Characterization. The products were characterized by XRD, SEM, TEM, HR-TEM, and FT-IR measurements. XRD measurements were performed on a Rigaku D/max 2500 diffractometer with Cu Kα radiation (λ= 0.154056 nm) at V= 40 kV and I = 150 mA, and the scanning speed was 6°/min. Morphology observations were performed on a Hitachi S4800 field emission scanning electron microscope (FE-SEM). TEM and HR-TEM images were recorded with a Tecnai G2 20S-Twin transmission electron microscope operating at an accelerating voltage of 120 kV. The pore diameter and the pore size distributions were determined by the Barrett–Joyner–Halenda (BJH) method. The specific surface areas (SBET) of the samples were calculated following the multipoint BET procedure.

Electrochemical Test. Electrochemical studies were characterized in CR2025-type coin cell with a multi-channel current static system Arbin (Arbin Instruments BT 2000, USA). The working electrodes were prepared by a slurry coating method on a aluminum foil with 75 wt% active

materials, 15 wt% acetylene black, and 10 wt% polyvinylidene fluoride (PVDF) dispersed in *N*-methyl-2-pyrrolidone (NMP). Test cells were assembled in an argon-filled glove box with water and oxygen contents less than 1 ppm using Li foil as the combined reference and counter electrode and polypropylene film (Celgard 2400) as separator. The electrolyte was 1 M $LiPF_6$ in a 1:1 (V/V) mixture of ethylene carbonate (EC) and dimethyl carbonate (DMC). The cells were galvanostatically discharge-charged at a constant current density of 0.1 C (1 C = 170 mA g^{-1}) based on the weight of LFP sample between 2.6 and 4.2 V at the room temperature. Electrochemical impedance spectroscopy (EIS) was also performed on the electrochemical workstation. The frequency of EIS ranged from 100 kHz to 0.1 Hz at the open-circuit potential.

S2. Results and Discussion

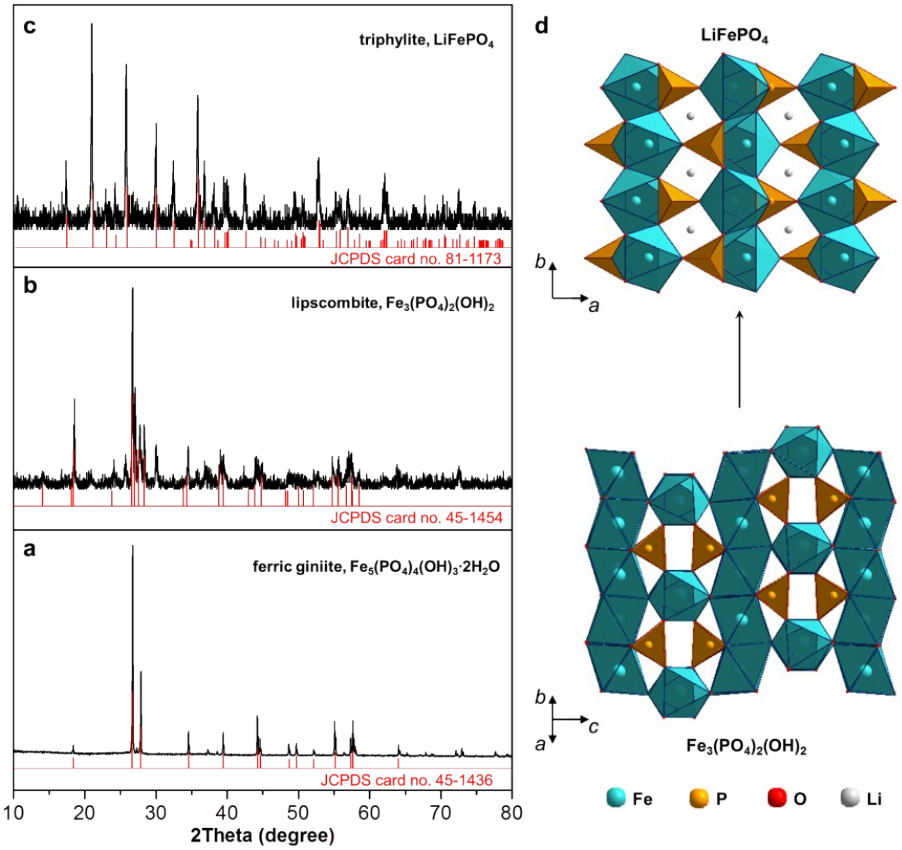

Figure S1. (a-c) XRD patterns of the samples obtained from different reaction time: (a) starting material, ferric giniite $Fe_5(PO_4)_4(OH)_3{\cdot}2H_2O$; (b) 4 h, mixture of lipscombite $Fe_3(PO_4)_2(OH)_2$ (major) and triphylite $LiFePO_4$ (minor); (c) 48 h, triphylite $LiFePO_4$. (d) Crystal structures of lipscombite $Fe_3(PO_4)_2(OH)_2$ and triphylite $LiFePO_4$.

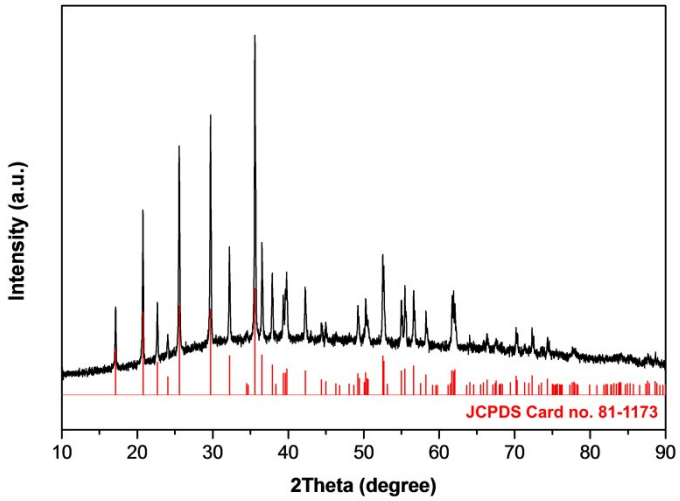

Figure S2. XRD pattern of LFP mesocrystals obtained at 700 °C without ionic liquid.

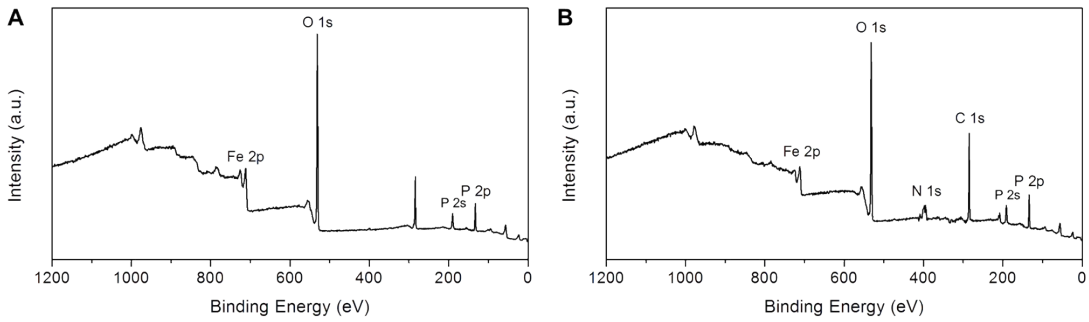

Figure S3. The wide XPS spectra of (A) ferric giniite, and (B) C,N-LFP mesocrystals.

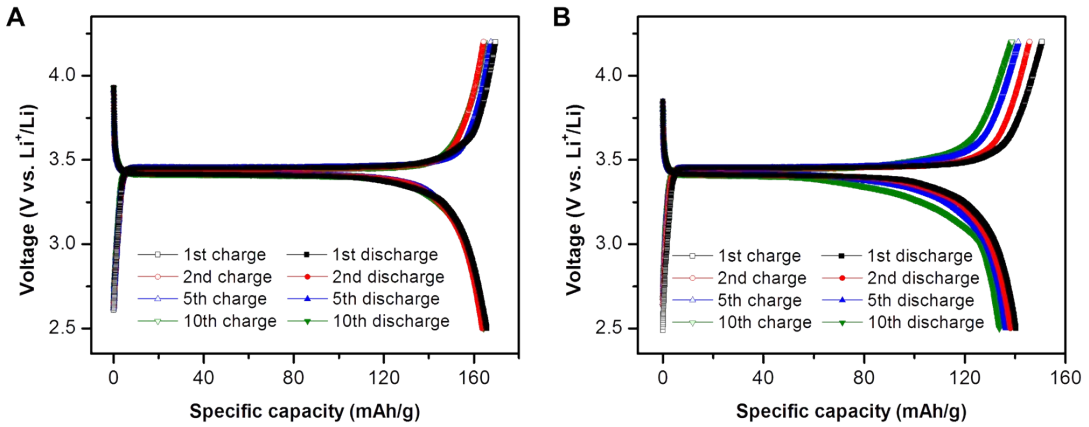

Figure S4. Charge/discharge profiles of (A) C,N-LFP mesocrystals, and (B) LFP mesocrystals at 0.1 C.

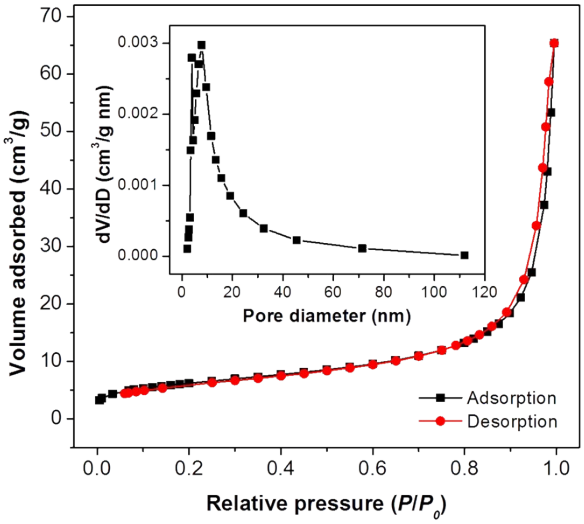

Figure S5. Nitrogen adsorption/desorption isotherms and the corresponding pore size distribution for the C,N-LFP mesocrystals. The BET surface area is about 21.96 m^2/g.

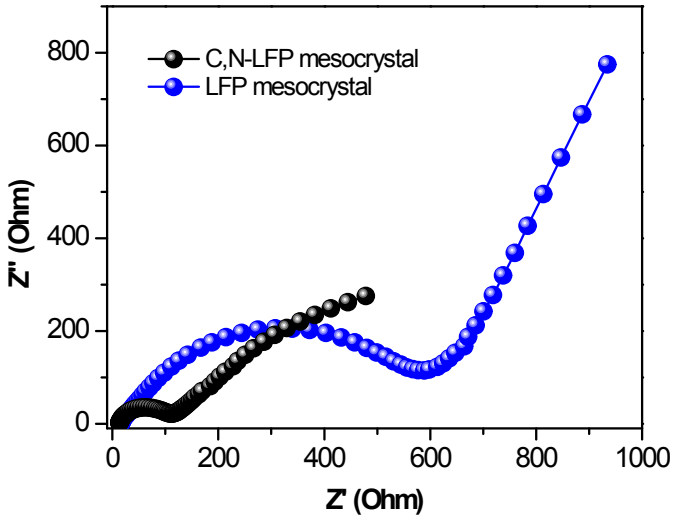

Figure S7. Impedance spectra (Nyquist plots) of the C,N-LFP mesocrystals and LFP mesocrystals collected in charged state.

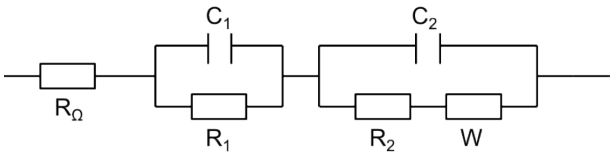

Figure S8. The simplified equivalent circuit of C,N-LFP mesocrystals and LFP mesocrystals.

Table S1. The fitting values of the resistance components in the simplified equivalent circuit.

Components	R_Ω/Ω	R_1/Ω	R_2/Ω	R_{total}/Ω
C,N-LFP mesocrystal	8.48	22.78	84.13	115.39
LFP mesocrystal	13.36	149.47	426.29	589.12

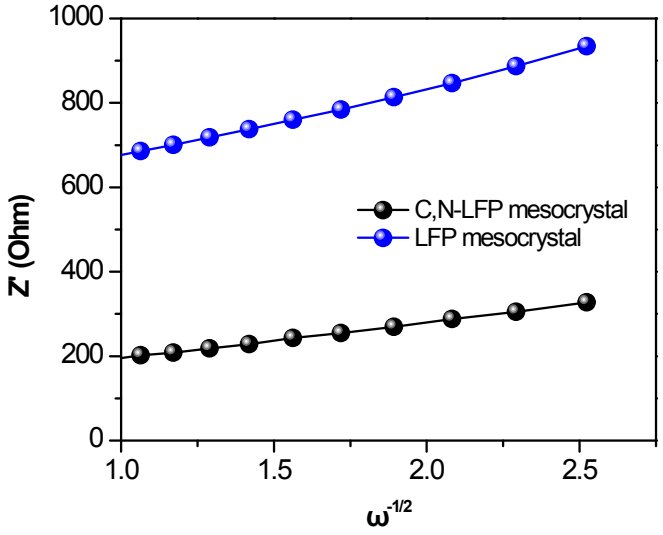

Figure S9. The real part of the complex impedance versus the reciprocal square root of the angular frequency in the low-frequency region at open circuit voltage for C,N-LFP mesocrystals (black) and LFP mesocrystals (bule).

Table S2. Summary of the preparation and electrochemical performance of LFP microstructures with different morphologies.

Synthesis	Structure	Capacity (mAh/g)	Ref.
solvothermal and thermal treatment	urchin-like LFP/C mesocrystals	100 (0.1 C) 40 (5 C)	2
solvothermal and thermal treatment	dumbbell-shaped LFP/C mesocrystals	143 (0.1 C) 84 (5 C)	3
solvothermal and thermal treatment	dumbbell-shaped LFP mesocrystals	140 (0.1 C) 38 (5 C)	3
solvothermal and thermal treatment	flower-like LFP/C mesocrystals	161 (0.1 C) 66 (5 C)	4
solvothermal and thermal treatment	flower-like LFP mesocrystals	147 (0.1 C) 17 (5 C)	4
microwave-assisted synthesis	plate-like LFP mesocrystals	148 (0.5 C)	5
hydrothermal and thermal treatment from	flower-like LFP/C microstructures	156 (0.1 C)	6

ferric giniite			
catalyst-assisted method	graphene embedded LFP nanoparticles	153 (0.1 C) 82 (5 C)	7
solvothermal method	LFP nanocrystals	105 (0.1 C)	8
seed growth method	porous and coarse LFP microstructures	155 (0.1C) 100 (5C)	9
sol-gel and thermal treatment	hierarchical LFP/nitrogen-doped carbon nanotube porous composite	140 (0.1 C) 78 (5 C)	10
solvothermal and thermal treatment	hierarchical C,N-LFP mesocrystals	159.6 (0.1 C) 102.8 (5 C)	This work

References

[1] Duan, X., Li, D., Zhang, H., Ma, J., Zheng, W. Crystal-Facet Engineering of Ferric Giniite by Using Ionic-Liquid Precursors and Their Enhanced Photocatalytic Performances under Visible-Light Irradiation. *Chemistry–A European Journal,* 2013, *19,* 7231-7242.

[2] Popovic, J., Demir‐Cakan, R., Tornow, J., Morcrette, M., Su, D. S., Schlögl, R., Titirici, M. M. $LiFePO_4$ Mesocrystals for Lithium−Ion Batteries. *Small*, 2011, *7*(8), 1127-1135.

[3] Zhou, N., Wang, H. Y., Uchaker, E., Zhang, M., Liu, S. Q., Liu, Y. N., Cao, G. Additive-free solvothermal synthesis and Li-ion intercalation properties of dumbbell-shaped $LiFePO_4$/C mesocrystals. *Journal of Power Sources*, 2013, *239*, 103-110.

[4] Zhou, N., Uchaker, E., Wang, H. Y., Zhang, M., Liu, S. Q., Liu, Y. N., Li, H. Additive-free solvothermal synthesis of hierarchical flower-like $LiFePO_4$/C mesocrystal and its electrochemical performance. *RSC Advances*, 2013, *3*(42), 19366-19374.

[5] Bilecka, I., Hintennach, A., Djerdj, I., Novák, P., Niederberger, M. Efficient microwave-assisted synthesis of $LiFePO_4$ mesocrystals with high cycling stability. *Journal of Materials Chemistry*, 2009, *19*(29), 5125-5128.

[6] Yang, Z., Zhang, J., Wu, Q., Zhang, W., Wang, H. Hydrothermal synthesis of $Fe_5(PO_4)_4(OH)_3{\cdot}2H_2O$ microflowers for fabricating high-performance $LiFePO_4$/C composites. *Ionics*, 2014, *20*(5), 653-658.

[7] Kim, W., Ryu, W., Han, D., Lim, S., Eom, J., Kwon, H. Fabrication of graphene embedded $LiFePO_4$ using a catalyst assisted self assembly method as a cathode material for high power lithium-ion batteries. *ACS applied materials & interfaces*, 2014, *6*(7), 4731-4736.

[8] Zhu, J., Fiore, J., Li, D., Kinsinger, N. M., Wang, Q., DiMasi, E., Kisailus, D. Solvothermal synthesis, development, and performance of $LiFePO_4$ nanostructures. *Crystal Growth & Design*, 2013, *13*(11), 4659-4666.

[9] Han, D. W., Ryu, W. H., Kim, W. K., Lim, S. J., Kim, Y. I., Eom, J. Y., Kwon, H. S. Tailoring Crystal Structure and Morphology of $LiFePO_4$/C Cathode Materials Synthesized by Heterogeneous Growth on Nanostructured $LiFePO_4$ Seed Crystals. *ACS applied materials & interfaces*, 2013, *5*(4), 1342-1347.

[10] Yang, J., Wang, J., Li, X., Wang, D., Liu, J., Liang, G., Sun, X. Hierarchically porous $LiFePO_4$/nitrogen-doped carbon nanotubes composite as a cathode for lithium ion batteries. *Journal of materials chemistry*, 2012, *22*(15), 7537-7543.